ISSN 1063-7834, Physics of the Solid State, 2013, Vol. 55, No. 1, pp. 81–87. © Pleiades Publishing, Ltd., 2013.
Original Russian Text © S.S. Aplesnin, A.M. Khar'kov, 2013, published in Fizika Tverdogo Tela, 2013, Vol. 55, No. 1, pp. 69–74.

MAGNETISM

Magnetic and Dynamic Properties of $Sm_xMn_{1-x}S$ Solid Solutions

S. S. Aplesnin[a, b, *] and A. M. Khar'kov[b, **]

[a] *Kirensky Institute of Physics, Siberian Branch of the Russian Academy of Sciences, Akademgorodok 50–38, Krasnoyarsk, 660036 Russia*

** e-mail: apl@iph.krasn.ru*

[b] *Reshetnev Siberian State Aerospace University, pr. im. Gazety "Krasnoyarskii Rabochii" 31, Krasnoyarsk, 660014 Russia*

*** e-mail: khark.anton@mail.ru*

Received June 6, 2012

Abstract—The real and imaginary parts of the magnetic permeability at frequencies of 0.1, 1.0, and 10.0 kHz, as well as the electron paramagnetic resonance (EPR) line width and *g*-factor, have been measured in $Sm_xMn_{1-x}S$ ($0.10 < x < 0.25$) solid solutions in the temperature range 5–300 K. The logarithmic dependence of the maximum in the imaginary part of the magnetic permeability on the frequency and the power-law dependence of Im μ on the temperature have been determined. The mechanism of relaxation of the magnetic moment in the magnetically ordered and paramagnetic phases has been established. The experimental results have been explained in terms of the Heisenberg model with competing exchange interactions and the formation of the antiaspiromagnetic state at low temperatures.

DOI: 10.1134/S1063783413010046

1. INTRODUCTION

At present, much attention has been paid to the study of materials with a strong correlation between the electrical and magnetic properties due to the practical interest in the development of the element base of microelectronics [1, 2]. Of special interest from the viewpoint of basic research are compounds containing variable valence elements, which undergo metal–insulator phase transitions and magnetic phase transformations, including variations in the magnetic properties with retaining the magnetic symmetry.

Among these compounds are EuS [3, 4] and SmS [5, 6]. Rare-earth elements Eu^{2+} and Sm^{2+} have no electrons in 5*d* orbitals, and their electronic configurations (except for 4*f* orbitals) are similar to configurations for alkaline-earth metals. The 4*f* and 5*d* orbitals with relatively close energies are responsible for specific properties exhibited by compounds containing these elements [7].

The divalent samarium ion Sm^{2+} has an isoelectronic configuration similar to that of the europium ion Eu^{3+} and undergoes a transition with the energy $E_{fd} = 0.18$ eV from the $4f^6$ state to the $4f^5(^6H)5dt_{2g}$ state [8]. The band gap E_g between the valence band and the conduction band in SmS is slightly smaller than that in MnS [9]. Under an external pressure $P \sim 6.5$ kbar, the SmS lattice undergoes strong compression, so that the unit cell parameter becomes equal to $a = 5.69$ Å, the electrical resistance decreases by one order of magnitude, the volume decreases by 13%, and the magnetic susceptibility is reduced by 60% [5, 10]. According to Deen et al. [10], these changes are associated with the transition of the samarium ion from the divalent state to the trivalent state.

The divalent ions $4f^6$ exist in the singlet ground state $J = 0$ and the triplet excited state $J = 1$, which is 30 meV higher in energy. Using inelastic neutron scattering, the dispersion of singlet–triplet excitations was determined as a function of the temperature, which confirms the thermal dynamics of the singlet–triplet model [11]. A decrease in the energy of singlet–triplet excitations at low temperatures, as compared to the free Sm^{2+} ion, was observed in Raman scattering [12]. This is associated with the exchange interactions between nearest neighbor samarium ions, as well as with the decrease in the splitting due to the spin–orbit interaction. A similar result was obtained from the Van Vleck paramagnetic susceptibility and expressed in the form $\chi = 8N\mu^2/E(T)$, where $E(T)$ is the singlet–triplet gap, which depends on the temperature, and N_s is the spin density [13]. The magnetic susceptibility of the trivalent samarium ion Sm^{3+} is of less importance as compared to the divalent samarium ion Sm^{2+} [3].

The long-range magnetic order in SmS, according to the nuclear magnetic resonance data and measurements of the specific heat at high pressure [14, 15], is formed at a pressure of 2.0 GPa.

It is assumed that the transformation of SmS into the trivalent state occurs at a sufficiently high pressure with the formation of a long-range magnetic order, because Sm^{3+} is a Kramers ion. This is confirmed by the measurements of X-ray absorption spectra in SmS

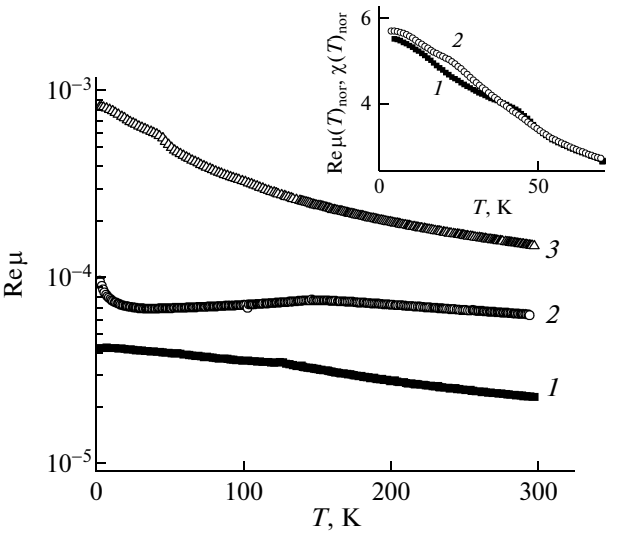

Fig. 1. Temperature dependences of the real part of the magnetic permeability Reμ at a frequency $f = 10$ kHz for $Sm_xMn_{1-x}S$ samples with x = (*1*) 0.10, (*2*) 0.20, and (*3*) 0.25. The inset shows the normalized values of (*1*) the magnetic permeability $Re\mu(T)_{nor} = Re\mu(T)/Re\mu(T = 290\ K)$ and (*2*) the magnetic susceptibility $\chi(T)_{nor} = \chi(T)/\chi(T = 290\ K)$ for $x = 0.25$ as a function of the temperature.

at a temperature of 4.5 K and a high pressure, where it was found that samarium has an intermediate valence of 2.8 at a pressure of 3.0 GPa [10].

Manganese and samarium sulfides have a face-centered cubic (fcc) crystal lattice of the NaCl type with the unit cell parameters $a = 5.222$ Å (MnS) [16] and $a = 5.965$ Å (SmS) [17], which dramatically decrease under pressure. It can be expected that, upon the substitution of samarium ions for manganese cations, the pressure produced by the nearest neighbors can induce electrons into the *d*-band and initiate a number of phase transitions (both magnetic and electric). The conduction band of manganese sulfide lies higher in energy than the conduction band of samarium sulfide. In the region of interaction between the elements Mn–Sm, there can occur a bending of the bands due to the exchange interaction and the existence of electrostatic forces between the manganese and samarium ions. Conduction electrons polarize spins of localized electrons of the manganese ions on the surface of samarium clusters. De Gennes calculated the paramagnetic Curie temperature in the *s–f* model in the molecular field approximation [18] and established its dependence on the concentration of conduction electrons.

The concentration of electrons in the conduction band is proportional to the ratio of ions $x = Sm^{3+}/Sm^{2+}$ divided by the number of degenerate states. The possible formation of ferromagnetic bonds also follows from the double-exchange model [19]. The analytical calculation of the phase diagrams of magnetic structures in the double-exchange model taking into account the indirect antiferromagnetic interaction (K) gives two phases in the range of electron occupation of the bands from 0.3 to 0.5. The canted ferromagnetic phase exists at $zKS^2/t > 0.4$, whereas the ferromagnetic state is observed at $zKS^2/t < 0.4$ [20]. For parameters $K \sim 0.001$ eV, $t = 0.1$–0.2, and $zKS^2/t \approx 0.1$, the ferromagnetic arrangement of the manganese spins was found near the samarium clusters.

The competition between ferromagnetic and antiferromagnetic interactions can lead to the formation of a new magnetic structure, for example, the spin glass or antiaspiromagnetic state, which has a long-range magnetic order in the longitudinal component of the spin with the "freezing" of the transverse spin projections.

The purpose of this work was to investigate the influence of a singlet–triplet transition in the mixed-valence regime on the magnetic properties of $Sm_xMn_{1-x}S$ compounds and to elucidate the mechanism of interaction between the spin, phonon, and electron subsystems.

2. SAMPLES AND EXPERIMENTAL TECHNIQUE

The $Sm_xMn_{1-x}S$ compounds were grown using the procedure described in [21]. The phase composition and crystal structure of the $Sm_xMn_{1-x}S$ samples were determined in the monochromatic CuK_α radiation on a DRON-3X diffractometer at a temperature of 300 K. According to the X-ray diffraction analysis, the $Sm_xMn_{1-x}S$ samples have an fcc crystal lattice of the NaCl type, which is similar to the lattice of the monosulfide α-MnS (antiferromagnet with $T_N = 150$ K). The specific magnetization was measured in a vacuum at temperatures of 5 and 50 K in magnetic fields up to 9 T. The magnetization of the samples in a magnetic field $H = 0.05$ T and the real and imaginary parts of the magnetic permeability at frequencies of 0.1, 1.0, and 10.0 kHz were measured on a Physical Property Measurement System (PPMS) in the temperature range $5\ K < T < 300\ K$.

3. EXPERIMENTAL RESULTS AND DISCUSSION

The real part of the magnetic permeability Reμ as a function of the temperature at a frequency $f = 10$ kHz for the $Sm_xMn_{1-x}S$ samples with $x = 0.10$, 0.20, and 0.25 is presented in Fig. 1. The investigation of the complex magnetic permeability $\mu = Re\mu + Im\mu$ makes it possible to determine the dynamic process of magnetization and the relaxation of the magnetic moment. The real part of the magnetic permeability at a frequency of 1 kHz and the magnetic moment in a field $H = 0.05$ T, divided by their values measured at

$T = 290$ K, are presented in the inset to Fig. 1. The temperature dependences of the magnetic permeability $\mathrm{Re}\mu/\mathrm{Re}\mu$ ($T = 290$ K) and the magnetization $M(T)/M(T = 290\ \mathrm{K})$ of the $Sm_xMn_{1-x}S$ compounds remain almost unchanged with variations in the concentration for the samples with $x = 0.1$ and 0.2; however, the difference is observed in the magnetic characteristics measured for the sample with $x = 0.25$ at $T < 40$ K in an external magnetic field and without the field.

The temperature T_g determined from the derivative of the real part of the magnetic permeability $d\mathrm{Re}\mu/dT$ increases by 3 K with an increase in the frequency from $f = 0.1$ to 10.0 kHz. The imaginary part of the magnetic permeability $\mathrm{Im}\mu$ has a maximum at the temperature T_g, which is shifted toward higher frequencies. This behavior is adequately described by the linear logarithmic dependence $T_g = 36.0 + 1.5\ln f$.

The imaginary part of the magnetic permeability $\mathrm{Im}\mu$ is almost independent of the temperature and tends to zero for the samples with $x = 0.1$ and 0.2 (Fig. 2). The measurement of the complex magnetic permeability gives important information about the dissipation of the energy of magnetic oscillations induced by an external alternating magnetic field. The dissipation of the magnetic moment is described by different functional dependences on the temperature and can be caused by the exchange interaction, magnetoelastic interaction, or interaction with delocalized electrons. These interactions determine three types of relaxation in semiconductors, namely, the spin–spin relaxation, the spin–lattice relaxation, and the relaxation due to the interaction of localized spins of the electrons with the band electrons. The low-frequency relaxation in the range 0.1–100.0 kHz is predominantly described by the longitudinal relaxation time, for which the temperature dependences $\tau(T)$ are found theoretically. The "paramagnet–long-range magnetic order" transition is accompanied by an enhancement of spin–spin correlations with the formation of a short-range magnetic order. As follows from the generally accepted theory of dynamic scaling, the relaxation time diverges as a power law with the correlation length ξ: $\tau = A\xi^z$, where z is the dynamic exponent. According to the static scaling hypothesis, $\xi \sim [(T/T_N) - 1]^{\nu}$, where ν is the critical exponent. These exponents depend on the dimension (of the system) and the number of components of the order parameter: in the Heisenberg model, $z = 1.5$; in the Ising model, $z = 2.175$ [22]; and for the spin glass, z and ν vary between 8 and 10 [23].

The superparamagnetic relaxation of the ideal system of noninteracting single-domain and magnetic nanoparticles is described by the Néel–Brown equation: $\tau = \tau_0 \exp(E_a/k_B T)$ [24]. Here, τ is the relaxation time at a given temperature, E_a is the energy required to change the orientation of the magnetic moment to opposite, and τ_0 is the frequency factor. On the other hand, the Vogel–Fulcher law $\tau = \tau_0 \exp(E_a/k_B(T - T_0))$ (where k_B is the Boltzmann constant, and τ_0 and T_0 are the constants related to the external frequency and the interaction force between the particles) gives the value in accordance with superparamagnetic behavior of the system of weakly interacting nanoparticles.

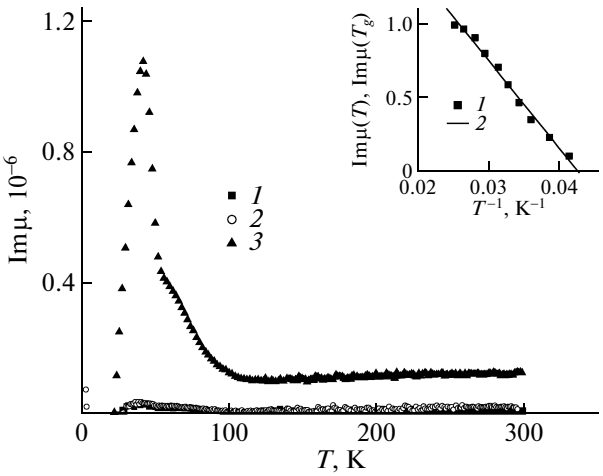

Fig. 2. Temperature dependence of the imaginary part of the magnetic permeability $\mathrm{Im}\mu$ for $Sm_xMn_{1-x}S$ samples with $x = (1)$ 0.10, (2) 0.20, and (3) 0.25 at a frequency $f =$ 10 kHz in an external field $H = 0$. The inset shows (1) the magnetic permeability of the $Sm_xMn_{1-x}S$ compound with $x = 0.25$ at a frequency $f = 10$ kHz, normalized to the quantity $\mathrm{Im}\mu(T_g)$ measured at a temperature T_g as a function of the inverse temperature and (2) the fitting function $\mathrm{Im}\mu(T) = 60\mathrm{Im}\mu(T_g)/T$.

The process of relaxation of the magnetic subsystem can occur through the lattice as a result of the magnetoelastic interaction in which the exchange energy depends on the distance between the ions. In the direct interaction of magnons and phonons, the relaxation time $1/\tau \sim (h\omega)^3 \coth(h\omega/k_B T)$ depends on the quasiparticle energy $h\omega$. The relaxation frequency rapidly increases in Raman scattering and is proportional to $1/\tau \sim T^9$ and T^7 for ions with even and odd numbers of $4f$ electrons, respectively [25]. The relaxation due to the conduction electrons occurs as a result of the exchange interaction with localized electrons, and the relaxation time is inversely proportional to the temperature: $1/\tau = \pi/h(I_{sd}N_E(E_F))^2 k_B T \approx 10^{10}(I_{sd}N_E(E_F))^2 T$, where $N_E(E_F)$ is the electronic density of states at the Fermi level [26]. The imaginary part of the magnetic permeability $\mathrm{Im}\mu$ is predominantly determined by the relaxation time $\mathrm{Im}\mu \sim \tau$. The dependence of the imaginary part of the magnetic permeability of the $Sm_xMn_{1-x}S$ solid solution on the reciprocal of the temperature is adequately described by the linear function $\mathrm{Im}\mu(T) = 60\mathrm{Im}\mu(T_g)/T$. The experimental data and fitting functions are presented in

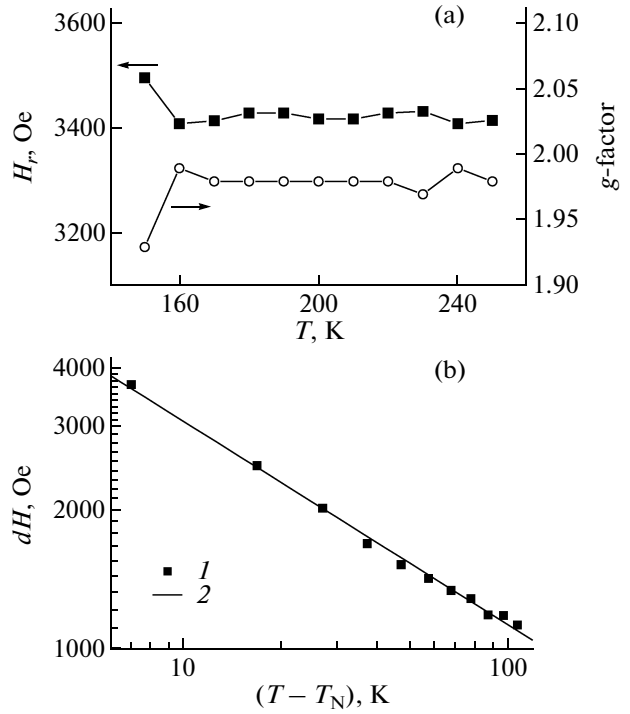

Fig. 3. (a) EPR resonance field H_r and the g-factor as a function of the temperature and (b) the line width dH as a function of the temperature difference $T - T_N$ for the composition with $x = 0.2$.

the inset to Fig. 2. A similar dependence of the relaxation time is observed for the spin glass CuMn [27].

This indicates that the interaction between localized and delocalized electron spins is responsible for the relaxation of the magnetic moment at low temperatures. The samarium ions induce electrons into the d-band, which leads to a ferromagnetic ordering between the nearest neighbor spins of the manganese ions.

The presence of Sm^{3+} impurities in the samples can be determined from electron paramagnetic resonance (EPR) measurements, because the Sm^{3+} ground state is the $\Gamma 7$ doublet. The averaged experimental value of the g-factor in all directions for the SmS crystal is $g = 0.70 + 0.02$ [28]. According to the EPR measurements carried out for the composition with $x = 0.2$, a single resonance is observed in the temperature range $150\ \text{K} < T < 300\ \text{K}$. The temperature dependences of the EPR resonance field H_r and the g-factor for the $Sm_{0.2}Mn_{0.8}S$ sample are shown in Fig. 3a. The g-factor does not depend on the temperature in the paramagnetic state and agrees well with the g-factor of MnS [16], which confirms the stability of the cubic lattice and the absence of distortions in the lattice of the $Sm_xMn_{1-x}S$ solid solutions. We did not reveal Sm^{3+} impurities in the $Sm_xMn_{1-x}S$ solid solutions. Therefore, the magnetic ordering can be associated with spins of the manganese ions.

The magnetic susceptibility is the integrated characteristic that depends on the spin–orbit and spin–lattice interactions. The temperature of the "long-range magnetic order–paramagnet" phase transition is difficult to determine from the temperature dependence of the magnetic susceptibility. Electron paramagnetic resonance makes it possible to determine the Néel temperature from the divergence of the line width in the vicinity of T_N. The mechanism of the relaxation of the magnetic moment in the gigahertz frequency range can be determined using the temperature dependence of the line width presented in Fig. 3b.

The EPR line width is adequately described by the power-law relationship $dH = A/(T - T_N)^\alpha$ with parameters $A = 8000$ and $\alpha = 0.44$. This relationship is consistent with theoretical calculations of $(T - T_N)^{-1/4}$ [26], which were performed in the molecular field approximation with the inclusion of the exchange and dipolar interactions. The difference in the exponents can be caused by different factors. The calculations disregard the magnetic field that causes a change in the spin–spin correlation function and its derivative. In addition, the molecular field approximation does not account for the spin correlations at the nearest neighbors. As a result, the exponents calculated for the spin–spin correlation function in the molecular-field and renormalization-group approximations differ from each other.

It is necessary to note that the line width in the MnF_2 antiferromagnet is described by a power-law function $(T - T_N)^{-3/8}$ [29] in zero magnetic field. Based on the experimental data, it is concluded that the spin relaxation in the $Sm_xMn_{1-x}S$ solid solutions in the temperature range $160\ \text{K} < T < 300\ \text{K}$ occurs as a result of the spin–spin interaction in comparison with which the spin–lattice contribution is small.

4. MODEL AND INTERPRETATION OF THE RESULTS

The magnetic structure of the $Sm_xMn_{1-x}S$ solid solution is formed by the exchange interaction between electrons of the manganese ions. The SmS compound is a Van Vleck paramagnet in the metal and semiconductor states. The direct hybridization of the $3t_{2g}$–$5t_{2g}$ electron orbitals of the samarium and manganese ions and the overlap of the t_{2g}–$3p$ electron orbitals of sulfur result in the formation of an impurity subband with the ferromagnetic exchange interaction between manganese spins on the surface of samarium clusters. Hereinafter, this interaction will be denoted by K. We calculate the magnetic characteristics in the

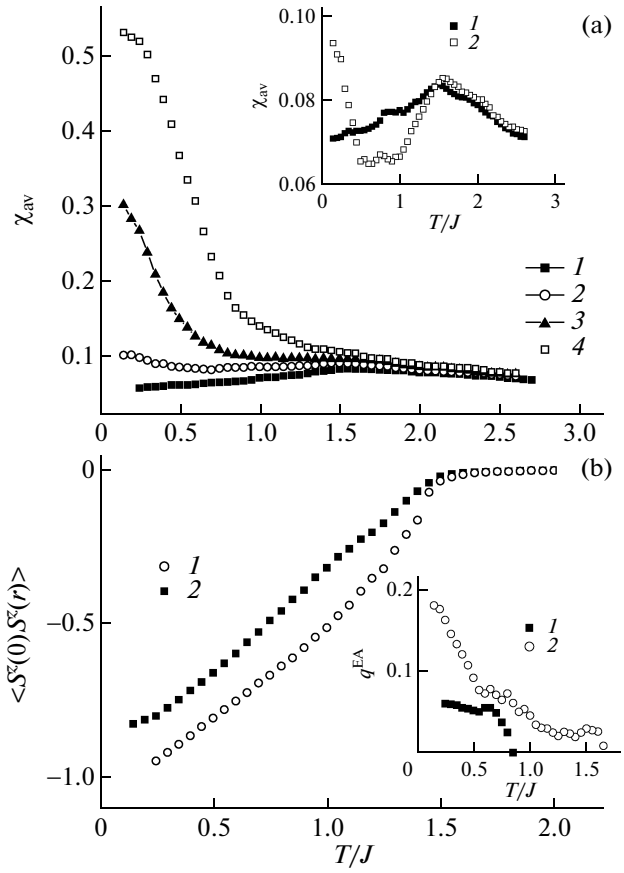

Fig. 4. (a) Temperature dependences of the magnetic susceptibility of the antiferromagnet with a random distribution of exchange interactions in the percolation region according to the Monte Carlo calculations with parameters $\lambda = K/|J| =$ (*1*) −0.5, (*2*) 0.5, (*3*) 1.0, and (*4*) 1.5. The inset shows the magnetic susceptibility of the antiferromagnet containing clusters with two and three sites with $S = 0$ and $\lambda = K/|J| =$ (*1*) 1 and (*2*) 2. (b) Temperature dependences of the spin–spin correlation function $\langle S^z(0)S^z(r = 5)\rangle$ in the antiferromagnet in the percolation region of empty sites with $\lambda = K/|J| =$ (*1*) −0.5 and (*2*) 1.0. The inset shows the Edwards–Anderson parameter q^{EA} for the antiferromagnet with $\lambda = K/|J| =$ (*1*) 1 and (*2*) 2 as a function of the temperature.

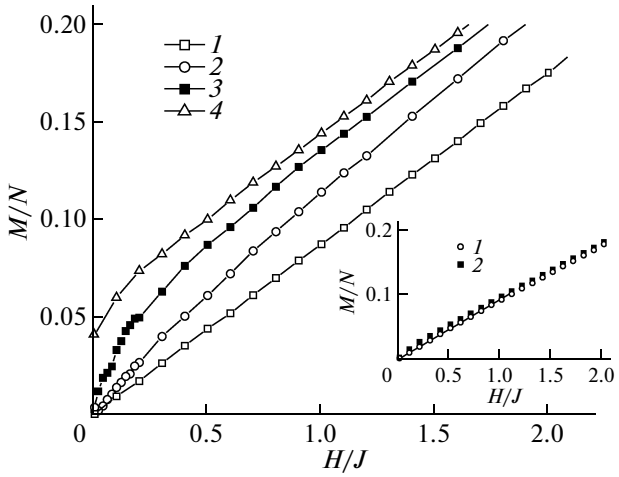

Fig. 5. Dependences of the magnetization on the magnetic field in the antiferromagnet with a random distribution of exchange interactions in the percolation region according to the Monte Carlo calculations with parameters $\lambda = K/|J| =$ (*1*) −0.5, (*2*) 0.5, (*3*) 1.0, and (*4*) 1.5. The inset shows the magnetization of the antiferromagnet consisting of clusters with two and three sites with $S = 0$ and $\lambda = K/|J| =$ (*1*) 1 and (*2*) 2.

Heisenberg model with random interactions. The Hamiltonian has the form

$$H = -\sum_{ij} J_{i,j} S_i S_j \zeta_i \zeta_j - \sum_i H S_i \zeta_j, \qquad (1)$$

where H is the external magnetic field, and ζ_i are random numbers that follow the law of distribution

$$P(\zeta_i) = (1-x)\delta(\zeta_i - 1) + x\delta(\zeta_i),$$
$$P(J_{ij}) = I_{ij}\delta(\zeta_{i+h} - 1)\delta(\zeta_{j+h} - 1) \qquad (2)$$
$$+ K_{ij}\delta(\zeta_{i+h})\delta(\zeta_{j+h}).$$

For the calculation of the magnetic characteristics, we used the Monte Carlo (MC) method with the number of lattice sites $N = 18 \times 18 \times 18$, $22 \times 22 \times 22$ and the number of MC steps $M_{MC} = 50000$–100000 per site with periodic boundary conditions. The magnetic structure is analyzed using the spin–spin correlation function. The temperature, at which the spin correlation $\langle S^z(0)S^z(r = 5)\rangle$ tends to zero, is related to the Néel temperature. The magnetic susceptibility is calculated as the arithmetic average of the magnetization induced by an external magnetic field H/J ($H = 0.05$ T) directed along the axes (x, y, z): $\chi = (M_x/H_x + M_y/H_y + M_z/H_z)/3$. The order parameter in the spin glass is the Edwards–Anderson parameter [30], which is calculated in the form

$$q^{EA} = \frac{1}{N}\sum_i \left(\frac{1}{M_{MC}}\sum_k S_{i,k}^{x,y}\right)^2, \qquad (3)$$

where the index of the sum k is the thermodynamic average and the index i is the configurational average.

The thermodynamic characteristics are calculated for small concentrations in the case of percolation in a cubic lattice. For example, for $x = 0.1$, the concentration of clusters containing two and three empty sites is proportional to $x_2 = 0.04$ and $x_3 = 0.002$ with $S = 0$, respectively. The temperature behavior of the magnetic susceptibility for this case is shown in the inset to Fig. 4a for $\lambda = K/|J| = 1$ and 2. The maximum in the magnetic susceptibility is observed at the Néel temperature. An increasing susceptibility $\chi(T)$ at low temperatures in the antiferromagnet with $\lambda = 2$ is associated with the canted antiferromagnetic structure in the cluster. The external magnetic field rotates the magnetic moment of the cluster in the field, which is

responsible for the nonlinear dependence $M(H)$ in weak fields (see inset to Fig. 5).

We investigate the percolation of empty sites in the framework of the model assuming that the spin chain with $S = 0$ starts on one face of the cube, goes randomly through the cube, and comes out on the opposite or nearest face. The chain is surrounded by ferromagnetic exchange interactions. The magnetic susceptibility of the sample consisting of eight chains is presented in Fig. 4a for different parameters of the ferromagnetic exchange. The behavior of the magnetic susceptibility $\chi(T)$ differs from that characteristic of a typical antiferromagnet at $\lambda > 1$. The maximum in the dependence $\chi(T)$ vanishes, and the magnetic susceptibility increases with a decrease in the temperature. In this case, the long-range antiferromagnetic order is retained, which follows from the spin–spin correlation function shown in Fig. 4b. The quantity $|\langle S^z(0)S^z(r)\rangle|$ describing the antiferromagnetic correlations decreases, the transverse components of the spins are "frozen" in random directions, and the antiferromagnetic ordering is observed only along the longitudinal components of the spins. This state is identified as a antiaspiromagnetic state with the Edwards–Anderson parameter shown in the inset to Fig. 4b.

The dependence of the magnetization on the magnetic field is adequately described by a linear function for the antiferromagnet with $K < 0$ and becomes nonlinear when the exchange interaction changes sign ($K > 0$). The curves $M(H)$ are shown in Fig. 5. The uncompensated magnetic moment arises in the antiferromagnet when the ferromagnetic exchange interaction exceeds the antiferromagnetic interaction.

Based on the theoretical results, we can explain the temperature behavior of the dependences of the magnetic susceptibility and magnetization on the magnetic field, which were measured in the $Sm_xMn_{1-x}S$ solid solutions. For a random distribution of samarium ions in the lattice, the exchange interactions between manganese ions on the surface of the boundaries of samarium clusters (Mn–Sm) become ferromagnetic. The competition between the ferromagnetic and antiferromagnetic interactions results in the formation of a local noncollinear magnetic structure at samarium concentrations lower than the critical concentration. The percolation leads to an increase in the magnetic susceptibility at low temperatures. In the percolation region, there are domains with a canted antiferromagnetic ordering and frozen transverse spin components, which is responsible for the maximum in the relaxation of the magnetic moment at $T = 40$ K.

5. CONCLUSIONS

It has been found that, in the $Sm_xMn_{1-x}S$ compound with a samarium concentration $x = 0.25$, there exists a spin-glass state. The temperature associated with the maximum in the relaxation of the magnetic moment increases logarithmically with an increase in the frequency.

The relaxation of the magnetic moment is caused by the exchange interaction between localized and delocalized electrons at low temperatures and is well described by a hyperbolic function of temperature.

The substitution of samarium for manganese does not lead to a change in the g-factor; in the $Sm_{0.2}Mn_{0.8}S$ solid solution, a single resonance is observed in the temperature range $150\ \text{K} < T < 300\ \text{K}$. The spin relaxation determined from the EPR line width is associated with spin–spin interactions in the paramagnetic state. We have proposed a model with competing antiferromagnetic and ferromagnetic interactions on the surface of the samarium cluster. The magnetic characteristics calculated using the Monte Carlo method are in qualitative agreement with the experimental data.

ACKNOWLEDGMENTS

This study was supported by the Russian Foundation for Basic Research (project nos. 09-02-92001-NNS_a, 09-02-00554-a, and 11-02-98004-r_sibir'_a).

REFERENCES

1. W. Ehrenstein, N. Mazur, and J. Scott, Nature (London) **442**, 759 (2006).
2. S. S. Aplesnin, O. N. Bandurina, O. B. Romanova, L. I. Ryabinkina, A. D. Balaev, and E. V. Eremin, J. Phys.: Condens. Matter **22**, 226006 (2010).
3. A. V. Golubkov, E. V. Goncharova, V. P. Zhuze, G. M. Loginov, V. M. Sergeeva, and I. A. Smirnov, *Physical Properties of Rare-Earth Chalcogenides* (Nauka, Leningrad, 1973) [in Russian].
4. K. Syassen, Physica B (Amsterdam) **139**, 277 (1986).
5. P. Wachter, in *Handbook on the Physics and Chemistry of Rare Earths*, Ed. by K. A. Gschneidner, Jr., LeRoy Eyring, G. H. Lander, and G. R. Choppin (North-Holland, Amsterdam, 1994), Vol. 19, Chap. 132.
6. A. Svane, G. Santi, Z. Szotek, W. M. Temmerman, P. Strange, M. Horne, G. Vaitheeswaran, V. Kanchana, B. L. Petit, and H. Winter, Phys. Status Solidi B **241**, 3185 (2004).
7. Y. Tamura and A. Shibukawa, Jpn. J. Appl. Phys. **32**, 3187 (1993).
8. V. N. Antonov, B. N. Harmon, and A. N. Yaresko, Phys. Rev. B: Condens. Matter **66**, 165208 (2002).
9. S. S. Aplesnin, G. A. Petrakovskii, L. I. Ryabinkina, G. M. Abramova, N. I. Kiselev, and O. B. Romanova, Solid State Commun. **129**, 197 (2004).
10. P. P. Deen, D. Braithwaite, N. Kernavanois, L. Paolasini, S. Raymond, A. Barla, G. Lapertot, and J. P. Sanchez, Phys. Rev. B: Condens. Matter **71**, 245118 (2005).
11. S. M. Shapiro, R. J. Birgeneau, and E. Bucher, Phys. Rev. Lett. **34**, 470 (1975).
12. M. I. Nathan, F. Holtzberg, J. E. Smith, J. B. Torrance, and J. C. Tsang, Phys. Rev. Lett. **34**, 467 (1975).

13. R. J. Birgeneau, E. Bucher, L. W. Rupp, and W. M. Walsh, Phys. Rev. B: Solid State **5**, 3412 (1972).
14. A. Barla, J. P. Sanchez, Y. Haga, G. Lapertot, B. P. Doyle, O. Leupold, and R. Rüffer, Phys. Rev. Lett. **92**, 066401 (2004).
15. Y. Haga, J. Derr, A. Barla, B. Salce, G. Lapertot, I. Sheikin, K. Matsubayashi, N. K. Sato, and J. Flouquet, Phys. Rev. B: Condens. Matter **70**, 220406 (2004).
16. S. S. Aplesnin, L. I. Ryabinkina, G. M. Abramova, O. B. Romanova, A. M. Vorotynov, D. A. Velikanov, N. I. Kiselev, and A. D. Balaev, Phys. Rev. B: Condens. Matter **71**, 125204 (2005).
17. V. V. Kaminskii, N. V. Sharenkova, L. N. Vasil'ev, and S. M. Solov'ev, Phys. Solid State **47** (2), 225 (2005).
18. P. G. de Gennes, C. R. Hebd. Seances Acad. Sci. **247**, 1836 (1958).
19. M. Yu. Kagan, D. I. Khomskii, and M. V. Mostovoy, J. Phys.: Condens. Matter **7**, 4213 (1995).
20. P. G. de Gennes, Phys. Rev. **118**, 141 (1960).
21. S. S. Aplesnin, L. I. Ryabinkina, O. B. Romanova, V. V. Sokolov, A. Yu. Pichugin, A. I. Galyas, O. F. Demidenko, G. I. Makovetskii, and K. I. Yanushkevich, Phys. Solid State **51** (4), 698 (2009).
22. S. W. Lovesey, E. Balcar, and A. Cuccoli, J. Phys.: Condens. Matter **7**, 2615 (1995).
23. P. Granberg, J. Mattson, P. Nordblad, L. Lundgren, R. Stubi, J. Bass, D. L. Leslie-Pelecky, and J. A. Cowenand, Phys. Rev. B: Condens. Matter **44**, 4414 (1991).
24. W. F. Brown, Phys. Rev. **130**, 1677 (1963).
25. A. Abragam and B. Bleaney, *Electron Paramagnetic Resonance of Transition Ions* (Clarendon, Oxford, 1970), Chap. 10, p. 602.
26. R. M. White, *Quantum Theory of Magnetism* (Springer, Berlin, 1983), Chap. 5, p. 158.
27. H. Alloul, Phys. Rev. Lett. **42**, 603 (1979).
28. W. M. Walsh, E. Bucher, L. W. Rupp, and L. D. Longinotii, AIP Conf. Proc. **24**, 34 (1975).
29. J. C. Burgiel and M. W. Stranberg, J. Appl. Phys. **35**, 852 (1964).
30. S. F. Edwards and P. W. Anderson, J. Phys. F: Met. Phys. **5**, 965 (1975).

Translated by O. Borovik-Romanova